J Mol Model (2013) 19:5159–5170
DOI 10.1007/s00894-013-1995-5

ORIGINAL PAPER

First-principles study of the structural transformation, electronic structure, and optical properties of crystalline 2,6-diamino-3,5-dinitropyrazine-1-oxide under high pressure

Qiong Wu · Chunhong Yang · Yong Pan · Fang Xiang · Zhichao Liu · Weihua Zhu · Heming Xiao

Received: 24 July 2013 / Accepted: 4 September 2013 / Published online: 9 October 2013

Abstract Periodic first-principles calculations have been performed to study the effect of high pressure on the geometric, electronic, and absorption properties of 2,6-diamino-3,5-dinitropyrazine-1-oxide (LLM-105) under hydrostatic pressures of 0–50 GPa. Obvious irregular changes in lattice constants, unit-cell angles, bond lengths, bond angles, and band gaps showed that crystalline LLM-105 undergoes four structural transformations at 8, 17, 25, and 42 GPa, respectively. The intramolecular H-bonds were strong at pressures of 0–41 GPa but weakened in the range 42–50 GPa. The lengths of the intermolecular H-bonds (<1.47 Å) indicated that these H-bonds have covalent character and tend to induce the formation of a new twelve-membered ring. Analysis of the DOS showed that the interactions between electrons, especially the valence electrons, strengthen under the influence of pressure. The *p* states play a very important role in chemical reactions of LLM-105. The absorption spectrum of LLM-105 displayed more bands—as well as stronger bands—in the fundamental absorption region when the pressure was high rather than low. A new absorption peak due to O–H stretching appeared at 18.3 eV above 40 GPa, indicating that covalent O–H bonds and a new twelve-membered ring are present in LLM-105.

Q. Wu · C. Yang · Y. Pan · F. Xiang · Z. Liu · W. Zhu (✉) · H. Xiao
Institute for Computation in Molecular and Materials Science and Department of Chemistry, Nanjing University of Science and Technology, Nanjing 210094, China
e-mail: zhuwh@mail.njust.edu.cn

C. Yang
School of Chemical and Biological Engineering, Yancheng Institute of Technology, Yancheng 224051, China

Y. Pan
Department of Chemical Engineering, Nanjing College of Chemical Technology, Nanjing 210048, China

Keywords First-principles calculations · 2,6-Diamino-3,5-dinitropyrazine-1-oxide · High pressure · Structural transformation · Electronic structures

Introduction

Pyridine and pyrazine are six-membered heterocyclic compounds with one or two nitrogen atoms. Compared to their carbocyclic analogs, pyridine and pyrazine derivatives have higher nitrogen contents, which contribute to the good detonation performance and thermal stability shown by these compounds [1–7]. In addition, nitrogen-rich compounds release nitrogen when they combust or explode, which makes them environmentally friendly energetic compounds. Among the various pyridine and pyrazine derivatives known, 2,6-diamino-3,5-dinitropyrazine-1-oxide (LLM-105) (ρ=1.913 g/cm^3) is an outstanding, insensitive explosive with excellent physical properties and good safety characteristics and detonation properties that was first synthesized at Lawrence Livermore National Laboratory [8]. LLM-105 is 120 % as powerful as another famous extremely insensitive explosive, 1,3,5-triamino-2,4,6-trinitrobenzene (TATB). At the same time, it is a thermally stable (DSC=342 °C) and relatively insensitive energetic material (h_{50}=117 cm) that presents 85 % of the energy of HMX (octahydro-1,3,5,7-tetranitro-1,3,5,7-tetrazocine) [9, 10]. This combination of properties makes LLM-105 an attractive insensitive high explosive.

Many studies have been done on the synthesis and thermal stability of LLM-105 [11–14]. It is well known that many famous energetic materials show several crystalline phases at different pressures or temperatures; for example, hexahydro-1,3,5-trinitro-1,3,5-triazine (RDX) (α-, β-, and γ-phases) [15–19] and HMX (α-, β-, γ-, and σ-phases) [20–22]. However, studies on the effects of pressure and temperature on the structure of LLM-105 are scarce, and polymorphs of LLM-105 have not been reported. Recently, Gump et al. [13]

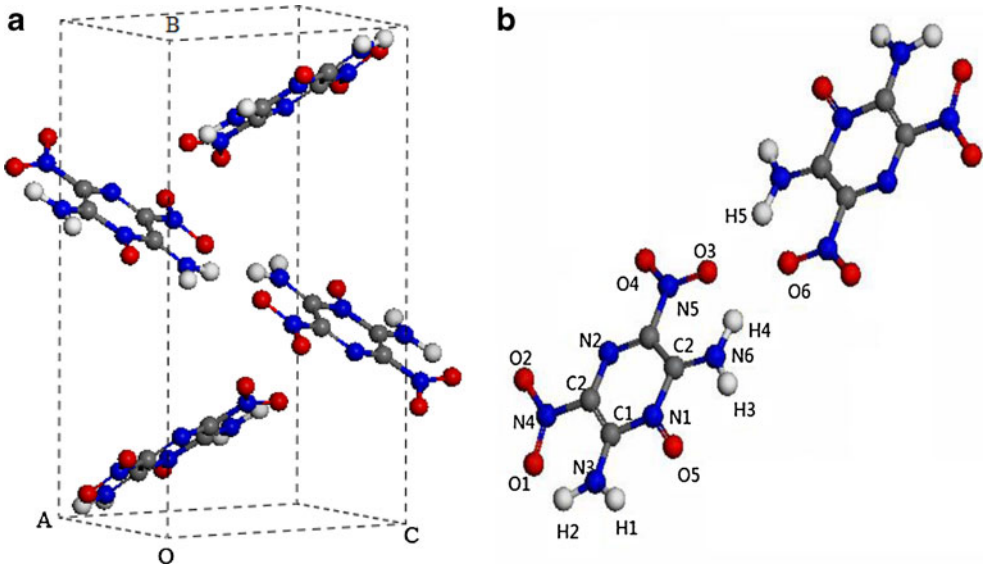

Fig. 1 Crystal and molecular structures of LLM-105

investigated the behaviorof LLM-105 at the high pressure of 5.4 GPa and a high temperature using synchrotron angle-dispersive X-ray diffraction experiments. However, at ambient temperature, at 373 K, and at 453 K, no phase change was observed, even when the measured pressure was increased to 5.4 GPa. This is may be because the pressure range 0–5.4 GPa is too narrow to observe such a phase transition. As we know, energetic compounds experience enormous pressure effects during the detonation process, and their decomposition processes are complicated and are still not well understood. In addition, the combination of amino groups and nitro groups in LLM-105 facilitates extensive hydrogen bonding, and these interactions can greatly influence its density and stability. These H-bonding interactions also vary depending on the conditions applied. Previous studies [23] have reported that these H-bonding interactions are similar to the phase transitions seen for 1,1-diamino-2,2-dinitroethylene (FOX-7) at high pressure. Thus, it is necessary to study the effects of pressure on H-bonding interactions in energetic compounds. As the phase transitions and hydrogen bonding presented by LLM-105 at different pressures are not currently well understood, there is a clear need to probe them at the atomic level.

It is a challenging task to experimentally measure the microscopic properties of energetic materials at high pressures. An alternative and complementary approach to experimental measurements is theoretical simulation, which is an effective way to model the physical and chemical properties of energetic solids at the atomic level. Recently, simulation methods based on density functional theory (DFT) using pseudopotentials and a plane-wave basis set have become well established, and have been successfully applied to study the structures and properties of energetic solids under hydrostatic compression [24–30].

In the study described in the present paper, we performed periodic DFT calculations to study the phase transitions, electronic structure, hydrogen bonds, and absorption properties of crystalline LLM-105 under hydrostatic pressures of 0–50 GPa. The positions of its atoms and its unit-cell parameters were allowed to relax to the minimum energy configuration in order to investigate its crystal structure at different pressures. Next, we examined the structure changes and hydrogen bonds under compression. Finally, we explored the effects of pressure on the absorption properties of LLM-105.

The remainder of this article is organized as follows. A brief description of our computational method is given in the following section. In the section after that, we present our results and discuss them. The final section of this paper provides a summary of our conclusions.

Table 1 Comparison of optimized lattice parameters for LLM-105 with experimental data at ambient pressure [a]

	a (Å)	*b* (Å)	*c* (Å)	β (°)	Cell volume
Expt.	5.709	15.844	8.416	101.14	740.06
LDA/CA-PZ	5.837(2.24)	15.579(−1.63)	8.221(−2.32)	99.51(−1.61)	737.24(−0.32)
GGA/PW91	6.008(5.24)	18.279(15.37)	8.706(3.45)	100.75(0.39)	939.23(26.91)

[a] Values in parentheses correspond to the percentage differences relative to the respective experimental data

Table 2 Calculated and experimental bond lengths (Å) and bond angles (°) for LLM-105

	LDA	Expt.		LDA	Expt.
N1–C1	1.381	1.368	N1–C1–C2	115.5	115.1
C1–C2	1.411	1.407	C1–C2–N2	123.6	124.3
C2–N2	1.310	1.315	C2–N2–C3	119.7	118.1
N2–C3	1.308	1.314	N2–C3–C4	123.0	123.6
C3–C4	1.427	1.406	C3–C4–N1	115.5	115.8
C4–N1	1.380	1.371	C4–N1–C1	122.6	122.9

Computational methods

The calculations performed in this study were done within the framework of DFT based on the CASTEP code [31], using Vanderbilt-type norm-conserving pseudopotentials [32] and a plane-wave expansion of the wavefunctions. The self-consistent ground state of the system was determined by using a band-by-band conjugate gradient technique to minimize the total energy of the system with respect to the plane-wave coefficients. The electronic wavefunctions were obtained using a density-mixing minimization method [33] for the self-consistent field calculation, and the structures were relaxed using the Broyden, Fletcher, Goldfarb, and Shanno (BFGS) [34] method. Geometry optimization involves reducing the magnitude of the calculated forces and stresses until they become smaller than predefined convergence tolerances. Therefore, it is possible to specify an external stress tensor to model the behavior of the system under tension, compression, shear, etc. In such cases, the internal stress tensor is iterated until it becomes equal to the applied external stress. The external stress is applied to the structure for geometry optimization, while the internal stress of the structure is accounted for by performing a stress tensor calculation. The LDA functional proposed by Ceperley and Alder [35] and parameterized by Perdew and Zunger [36] (named CA-PZ) was employed. The cutoff energy of plane waves was set to 550 eV. Brillouin zone sampling was performed using the Monkhorst–Pack scheme with a k-point grid of 2×1×2. The values of the kinetic energy cutoff and the k-point grid were determined to ensure total energy convergence.

To allow comparison with experiments, we used the crystal structure of LLM-105 at ambient pressure and temperature as the input structure. LLM-105 crystallizes in an orthorhombic lattice with a $P2_1/n$ space group, and contains four $C_4H_4N_6O_5$ molecules per unit cell [37]. Figure 1 displays the crystalline and molecular structure of LLM-105. In order to find a stable geometry, the experimental crystal structure of LLM-105 [37] was first relaxed to allow the ionic configuration, cell shape, and volume to change at ambient pressure. We then applied hydrostatic compression of 1–50 GPa to relax the crystal structure without any symmetry constraints. All of the calculations were performed for the same crystal structure of LLM-105. In the geometry relaxation, the total energy of the system was converged to a tolerance of less than 2.0×10^{-5} eV, the residual force was less than 0.05 eV/Å, the atomic displacement was less than 0.002 Å, and the residual bulk stress was less than 0.1 GPa. Previous studies employed the same approach to simulate the hydrostatic compression of other energetic crystals [38, 39], and the results obtained indicate that the calculated results are in agreement with those obtained experimentally.

Results and discussion

As a base and a benchmark for studying LLM-105, both LDA/CA-PZ and GGA/PW91 (Perdew–Wang 91) [40] were applied to fully relax the bulk LLM-105 at ambient pressure without any constraints. Table 1 lists the experimental and optimized cell parameters of LLM-105. It was found that the errors in the LDA results were much smaller than those in the GGA results. This shows that the LDA functional produces more reliable crystal structures, which is in agreement with the conclusions drawn from our previous studies on solid crystals [24–26]. We also note that, in Table 2, the internal structure parameters derived from the LDA/CA-PZ bond lengths and angles are close to those of the corresponding experimental data. These comparisons confirm that our computational parameters are reasonably accurate. Consequently, we used LDA/CA-PZ in subsequent calculations.

Crystal structure

Many experimental and computational studies have indicated that adjusting the external pressure may induce changes in molecular conformation, phase transitions, and the formation of more densely packed materials [24, 26, 41, 42]. The relaxed lattice constants (a, b, c) of the crystal structure of LLM-105 under different hydrostatic pressures are depicted in Fig. 2. It was found that, for a particular range of pressures, the lattice constants for LLM-105 vary in different ways.

The a-axis decreases rapidly in the pressure range 0–7 GPa but increases suddenly at a pressure of 8 GPa. After that, it decreases gradually until 10 GPa but then increases again until 13 GPa. Then it decreases gradually until 16 GPa but increases sharply at a pressure of 17 GPa. Afterwards, it decreases consistently in the pressure range 18–24 GPa but suddenly increases at a pressure of 25 GPa. Then it decreases gradually until 39 GPa before increasing slightly up to 41 GPa. Finally, it increases very markedly at 42 GPa and then decreases up to 50 GPa.

Overall, the b-axis gradually decreases with the increasing pressure, except that four prominent drops occur at pressures of 8, 17, 25, and 42 GPa, respectively. It drops by 1.17 %, 1.78 %, 0.94 %, and 1.59 %, respectively, at those pressures;

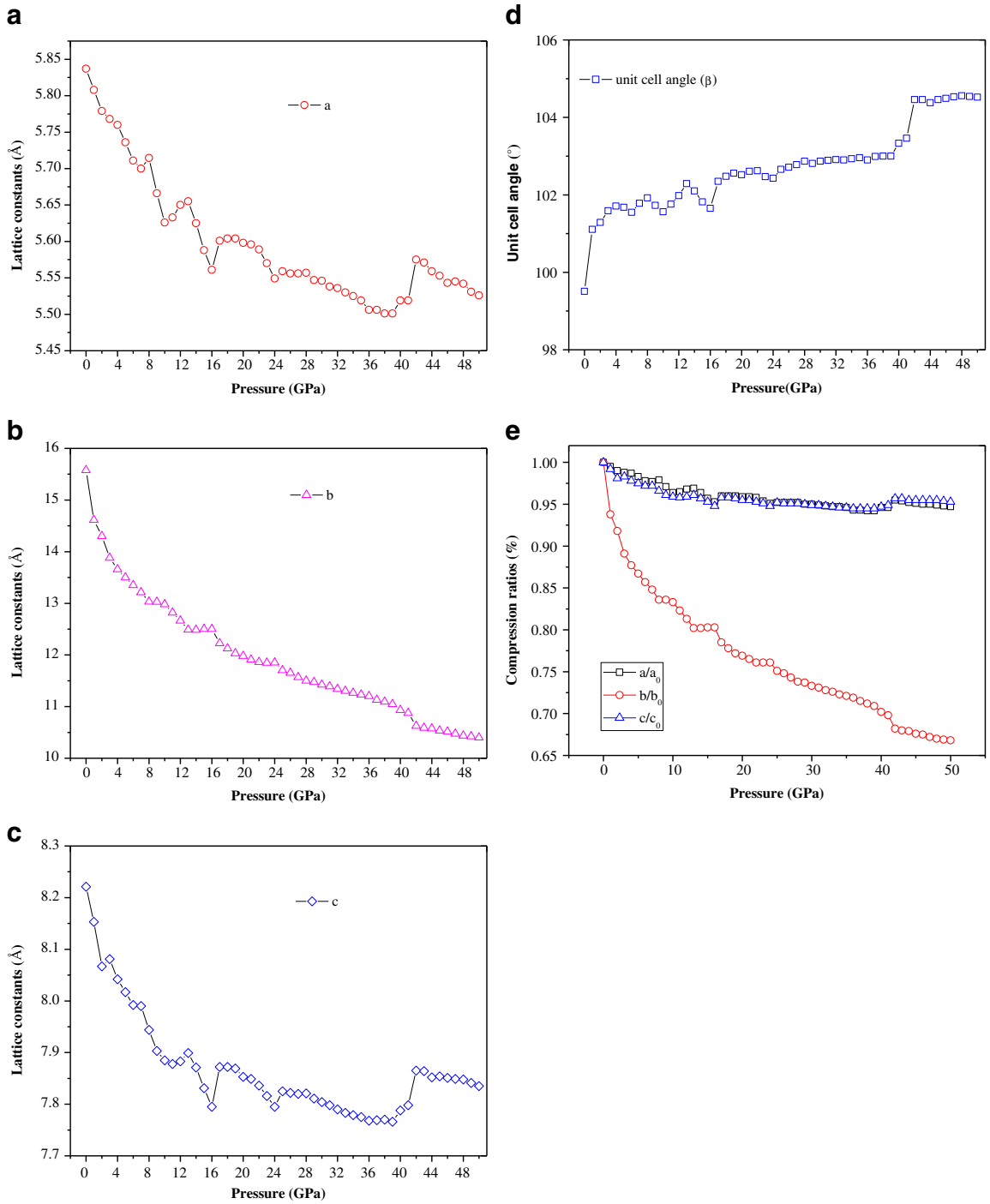

Fig. 2a–e Various parameters of LLM-105 as a function of pressure: **a–c** Lattice constants a, b and c, respectively; **d** unit-cell angle β; **e** compression ratios a/a_0, b/b_0, and c/c_0

these drops are much larger than those seen for the a-axis at 7 GPa (0.89 %) and 9 GPa (0.01 %), 16 GPa (0.01 %), 18 GPa (0.64 %), 24 GPa (0.01 %), 25 GPa (0.33 %), 41 GPa (0.37 %), and 43 GPa (0.25 %).

The c-axis gradually decreases in the pressure range 0–16 GPa, except that a small increase occurs at 3 GPa, some small fluctuations are seen at about 12 GPa, and the c-axis remains unchanged in the range 7–8 GPa. However, it also increases very obviously at 17 GPa, before decreasing in the pressure range 17–24 GPa but then increasing at 25 GPa. From 25 to 41 GPa, it gradually decreases, but it then increases markedly at 42 GPa before finally decreasing gradually up to 50 GPa. Overall, the lattice constants changed most irregularly at pressures of 8, 17, 25, and 42 GPa, indicating that four structural transitions may occur at these four pressures. The fluctuations in the lattice constants observed at

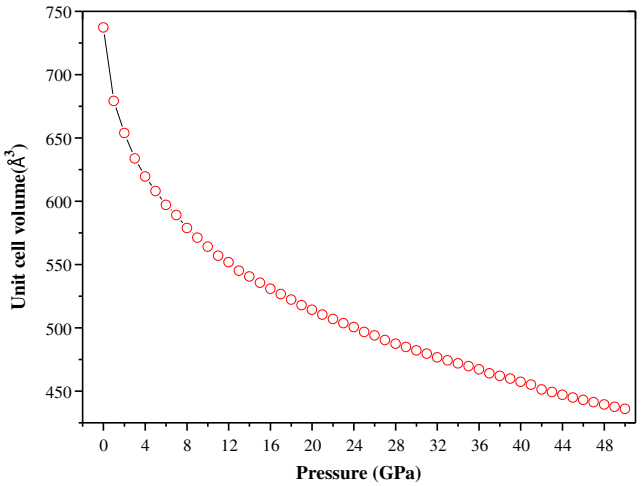

Fig. 3 Unit-cell volume of LLM-105 as a function of pressure

pressures of 8–16 GPa may suggest that the crystalline structure is unstable and compressible in this pressure range. Similar variation is observed in Fig. 2d, which shows the change in the unit-cell angle as a function of pressure for LLM-105. The unit-cell angle gradually increases with increasing pressure up to 50 GPa, except for four main fluctuations at 8–16 GPa, 17–24 GPa, 25–41 GPa, and 42–50 GPa, respectively. This indicates that four structural transitions occur at 8, 17, 25, and 42 GPa, respectively. The fluctuations seen in the pressure range 8–16 GPa indicate that the crystalline structure is not stable under compression. These pressure-induced changes in unit-cell angle agree with those observed for lattice constants.

The pressure-induced variations in the compression ratios of LLM-105 were also calculated and are shown in Fig. 2e. It is clear that the variations in the compression ratios for the *a*- and *c*-directions show similar trends, but they are quite different trends to that seen for the *b*-direction, which indicates that the compressibility of the LLM-105 crystal is anisotropic. In the pressure range 0–50 GPa, the compressibility in the *b*-direction is significantly greater than those in the *a*-direction and *c*-direction ($b > c \approx a$), which was also seen in previous studies in the pressure range 0–5.4 GPa [13]. The total compressions along the *a*-, *b*-, and *c*-directions in the pressure range 0–50 GPa are 5.33 %, 33.23 %, and 4.70 %, respectively. This means that the structure is much stiffer in the *a*- and *c*- directions than in the *b*-direction.

Figure 3 presents the variations in the unit cell volume of LLM-105 as a function of pressure. It is seen that the unit cell volume generally decreases with increasing pressure, and the total compression in the pressure range 0–50 GPa is 51.89 %. The total compression ratio of the unit cell volume in the pressure range 0–5 GPa is 16.9 %, which is close to that (15.2 %) seen at room temperature in [6]. This indicates that our results agree well with the experimental values. It is worth noting that the compression ratios of the unit cell volume at 8, 25, and 42 GPa are 1.75 %, 0.77 %, and 0.85 %, respectively, which are much higher than those at 7 GPa (1.32 %), 9 GPa (1.31 %), 24 GPa (0.60 %), 26 GPa (0.57 %), 41 GPa (0.46 %), and 43 GPa (0.46 %). This indicates that there are structural transitions at 8, 25, and 42 GPa, respectively, that prompt a decrease in volume. However, the scenario at 17 GPa is different. The compression ratios at 16, 17, and 18 GPa are 0.87 %, 0.80 %, and 0.82 %, respectively, which suggest that the structural transition at 17 GPa may cause the volume to increase slightly.

Molecular structure

Adjusting the pressure causes changes not only to the unit cell but also to the molecular geometry, such as bond lengths, bond angles, and torsion angles. The variations in the bond lengths of LLM-105 as a function of pressure are presented in Fig. 4. Figures 4a, b provide the variations in the lengths of all six C–N bonds and C–C bonds in the ring. Generally, as the pressure increases, the bond lengths decrease at different compression rates, and some obvious fluctuations occur due to structural transitions. In the pressure range 0–50 GPa, the bonds C3–C4 and N2–C3 decrease by about 0.054 and 0.005 Å, respectively. These decreases show that the shape of the ring changes significantly under compression. Some irregular changes in Figs. 4a, b are as follows. (i) At a pressure of 8 GPa, the lengths of the C4–N1 and C2–N2 bonds increase suddenly. (ii) At 17 GPa, the N2–C3 bond length increases while the C1–N2 bond length decreases dramatically. (iii) At 25 GPa, the N2–C3 bond length increases unexpectedly. (iv) At 42 GPa, the N2–C3, N1–C1, and C1–C2 bond lengths increase abruptly, while the C3–C4 bond length decreases greatly. These features suggest that there may be four structural transitions at these four pressures. Figures 4c, d present the variations in the lengths of the bonds associated with C–NH_2 (C1–N3 and C4–N6 bonds) and C–NO_2 (C2–N4 and C3–N5 bonds), respectively. The four C–N bonds gradually decrease with increasing pressure, except for several irregular changes caused by the structural transitions. For instance, the C1–N3 and C2–N4 bond lengths clearly increase at 8 and 42 GPa, respectively, while the C3–N5 bond length decreases sharply at 8, 17, and 42 GPa. In addition, the C3–N5 bond shortens by about 0.096 Å, which is more than the shortening of the N2–C3 bond (about 0.054 Å) and C4–N6 bond (about 0.05 Å) in the ring. This suggests that the bonds in C–NO_2 are more unstable than the other bonds in the ring and the bonds in C–NH_2. Thus, C–NO_2 fission may be the primary step in the decomposition of LLM-105. Figure 4g displays the variation in the length of the N–O bond in the ring as a function of pressure. It is found that the N1–O5 bond length gradually decreases, except for two obvious unexpected increases at 17 and 42 GPa caused by the structural transitions.

Previous studies [43] have reported that two kinds of intramolecular H-bonds are present in LLM-105: those between NH_2 and NO_2 and those between $(N)_{ring}$–O and NH_2. The intramolecular H-bond lengths were measured and are displayed in Fig. 4h. It is apparent that the H-bond lengths are 1.9–2.2 Å, which are in the range of normal Y…H separation (Y=F, O, or N atom), 1.5–2.2 Å [47]. Thus, all of the intramolecular H-bonds appear to be moderate ones. In addition, Fig. 4i displays the variations in the total length of the four H-bonds in LLM-105 as a function of pressure. It is found that the H-bonds shorten in the pressure range 0–41 GPa (the H-bonds are longest, 8.338 Å in total, at 1 GPa), but they increase beyond 8.338 Å at pressures of 42–50 GPa. Thus, according to the lengths of the intramolecular H-bonds, LLM-

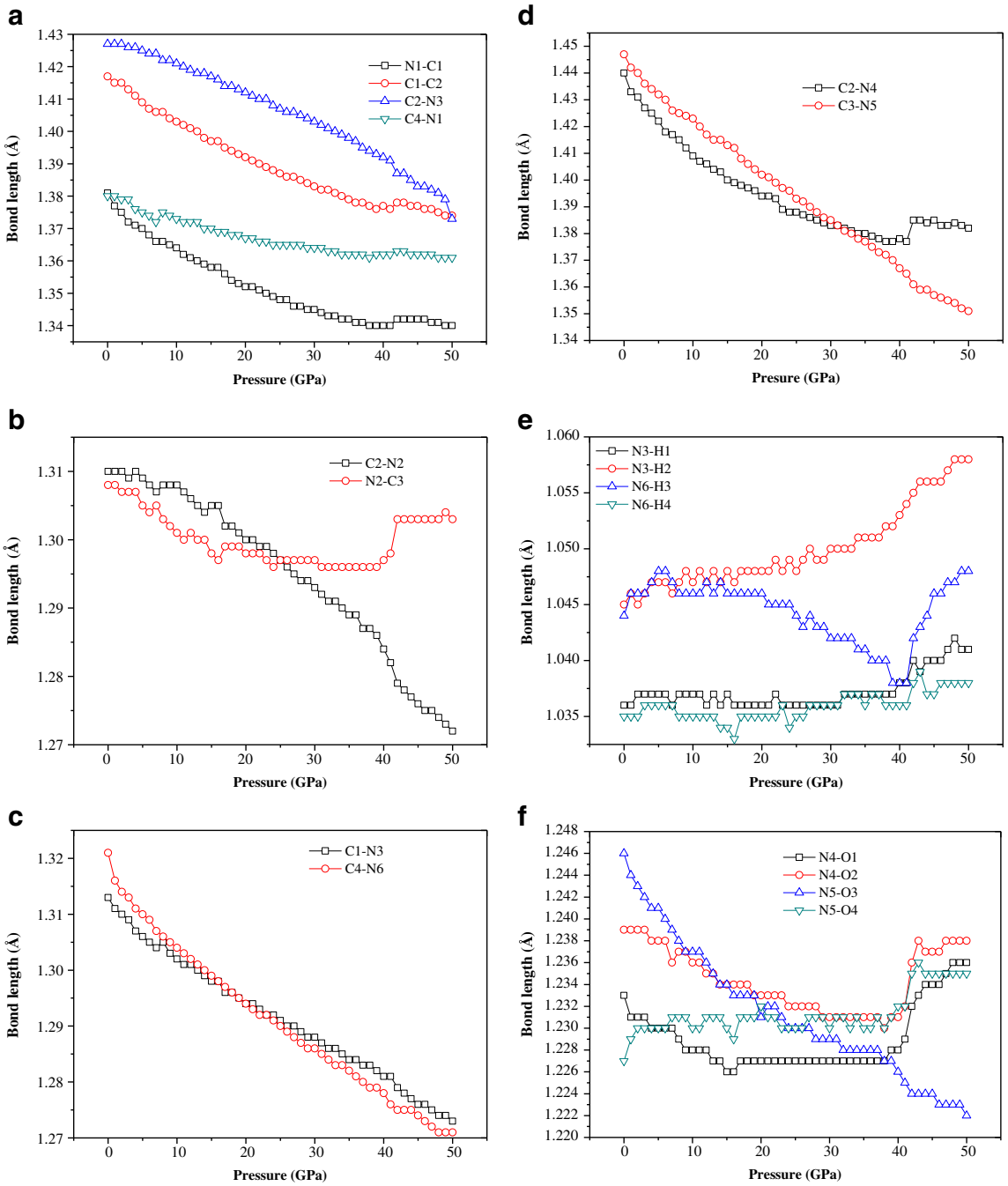

Fig. 4a–j Various bond lengths in LLM-105 as a function of pressure: **a** N1–C1, C1–C2, C2–N3, C4–N1; **b** C2–N2, N2–C3; **c** C1–N3, C4–N6; **d** C2–N4, C3–N5; **e** N3–H1, N3–H2, N6–H3, N6–H4; **f** N4–O1, N4–O2, N5–O3, N5–O4; **g** N1–O5; h O5–H1, O5–H3, O1–H2, O3–H4; **i** total H-bond length as a function of pressure; **j** length of O6–H4 in LLM-105 as a function of pressure

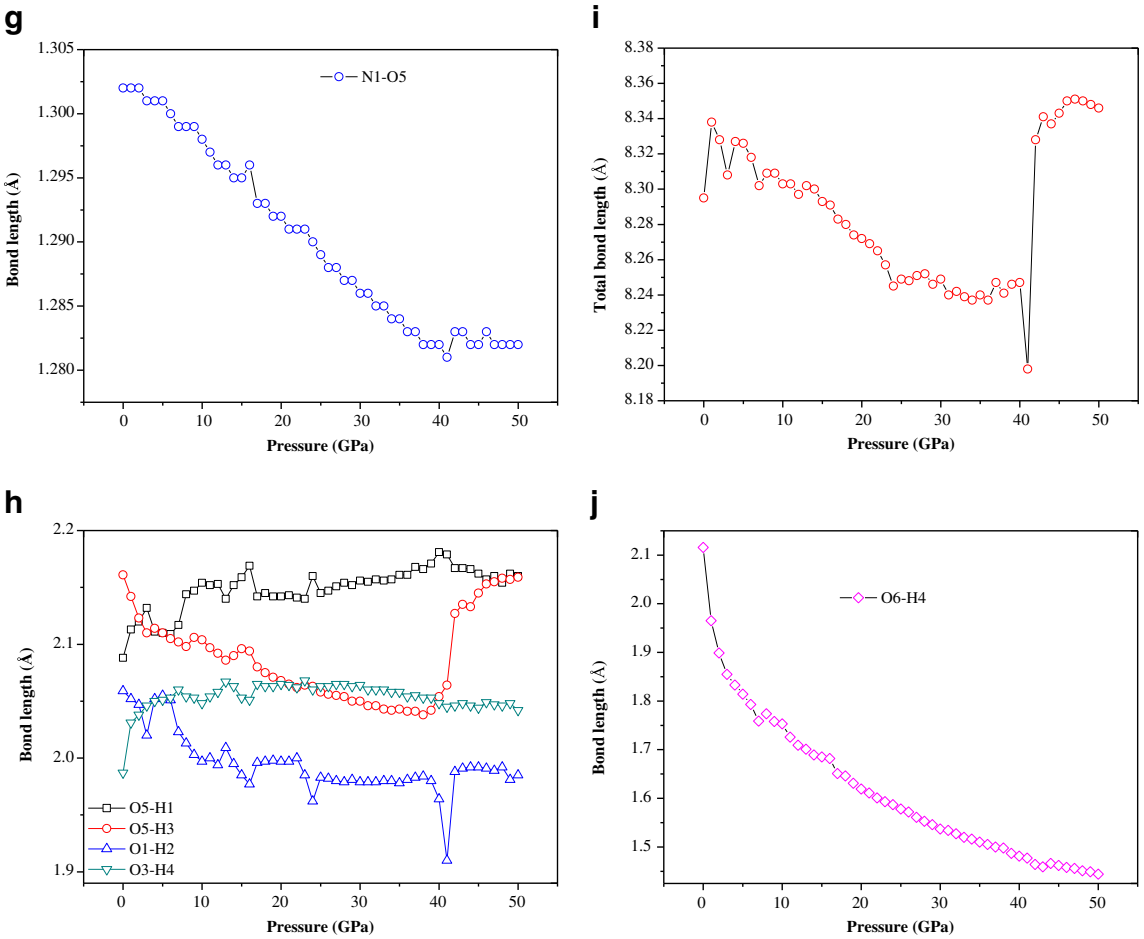

Fig. 4 (continued)

105 appears to have the weakest and strongest intramolecular H-bonds in the pressure ranges 42–50 GPa and 25–41 GPa, respectively. There are also intermolecular H-bonds in LLM-105. The lengths of the intermolecular H-bonds between NH_2 and NO_2 were measured and are displayed in Fig. 4j. The H5…O3 separation is equal to the H4…O6 separation, so we have only shown the H4…O6 separation. It is seen that the length of the intermolecular H-bond (H4…O6) decreases irregularly with increasing pressure, except for an increase and a significant drop at 8 and 17 GPa, respectively, which are caused by the structural transitions. This indicates that the intermolecular H-bond becomes stronger with increasing pressure. It should be noted that the intermolecular H-bond length in the crystalline structure at pressures of 42–50 GPa is below 1.47 Å, which is below the "normal" range 1.5–2.2 Å. This means that this intermolecular H-bond is unusually strong, and induces the formation of a new, large, twelve-membered ring, as shown in Fig. 5. This big ring becomes more and more stable with increasing pressure, which may make the molecule more stable. Thus, the intramolecular and intermolecular H-bonds in LLM-105 greatly improve its stability.

Figures 6a, b display the variations in the six bond angles in the ring as a function of pressure. It is clear that the bond angles vary in very different ways with increasing pressure. For example, in the pressure range 0–24 GPa, the angle C1–C2–N2 increases by more than 1.4°, while N2–C3–C4 decreases by about 0.06°, indicating that the ring deforms under compression. Also, because of the structural transitions, the trends for each angle at 8, 17, 25, and 42 GPa change irregularly. For instance, at 8 GPa, the angles C2–N2–C3 and C3–C4–N1 increase, while C4–N1–C1 decreases suddenly. At 16 GPa, the angles C2–N2–C3 and C4–N1–C1 increase, while C3–N4–N1 and C1–C2–N2 decrease abruptly. At 25 GPa, the angle C1–C2–N2 decreases suddenly. At 42 GPa, the angle C1–C2–N2 decreases significantly, while the angle C2–N2–C3 markedly increases. All of these irregular changes indicate that LLM-105 undergoes four structure transformations at 8, 17, 25, and 42 GPa, respectively. Figure 6c displays the variations in the $(C–N)_{ring}$–O angles (C1–N1–O5 and C4–N1–O5) as a function of pressure. The irregular changes seen for the angle C4–N1–O5 at 8, 17, 25, and 42 GPa present further

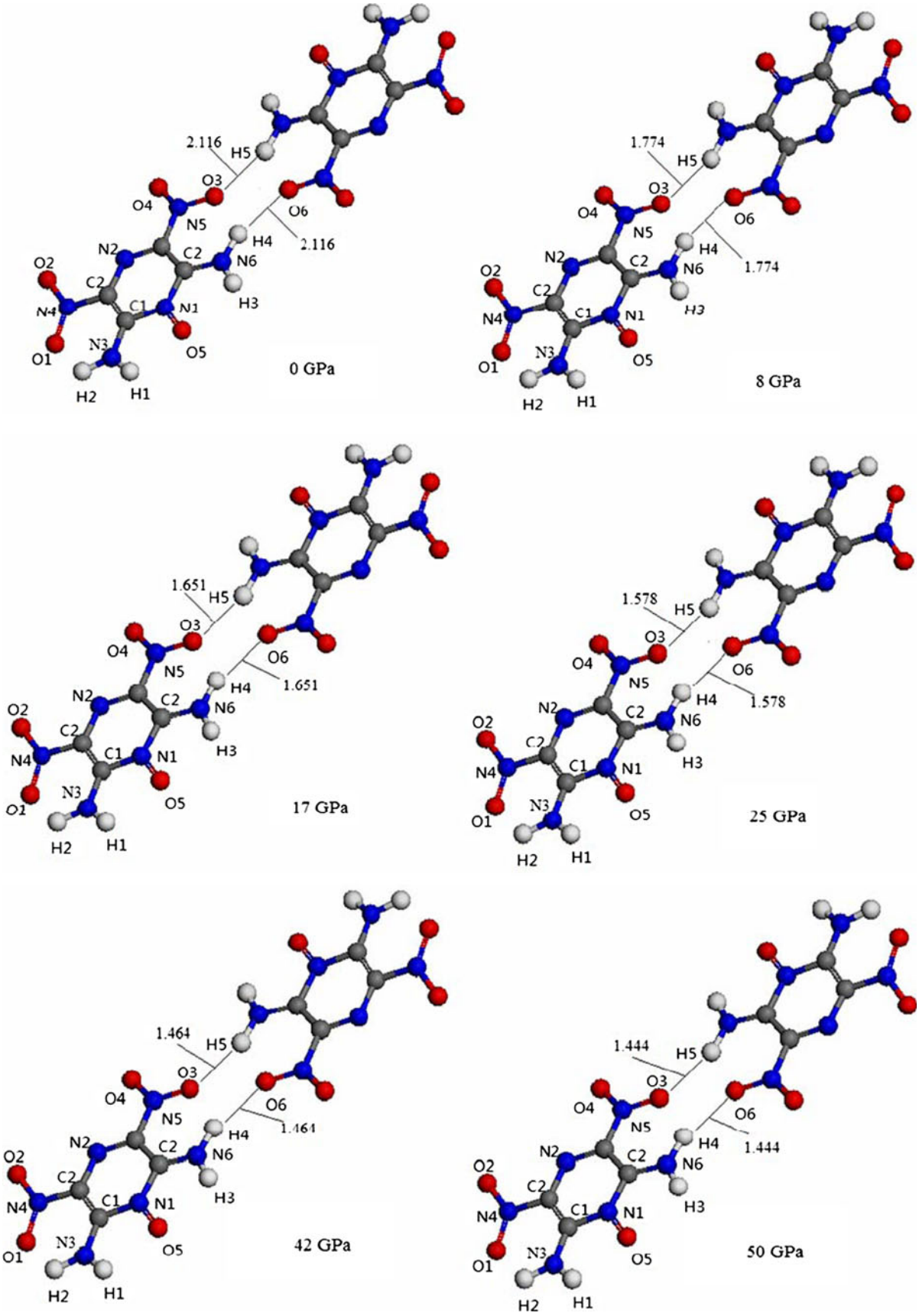

Fig. 5 Formation of a new twelve-membered ring

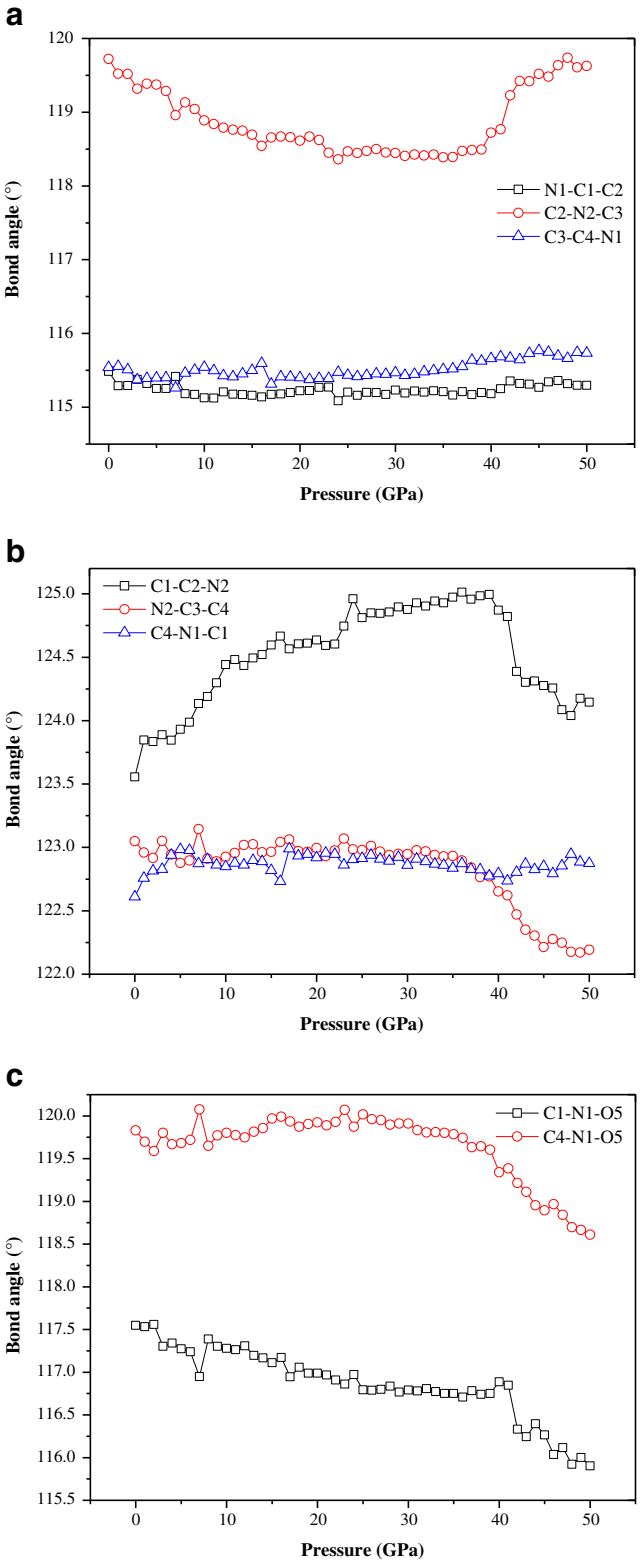

Fig. 6a–c Bond angles of LLM-105 as a function of pressure: **a** N1–C1–C2, C2–N2–C3, C3–C4–N1; **b** C1–C2–N2, N2–C3–C4, C4–N1–C1; **c** C1–N1–O5, C4–N1–O5

evidence that structural transitions occur at these four pressures.

Electronic structure

The band gap generally refers to the energy difference (in electron volts) between the top of the valence band and the bottom of the conduction band. Figure 7 displays the band gap of LLM-105 at different pressures. Overall, its band gap decreases with increasing pressure, except for two sharp drops at 17 and 41 GPa that are caused by structural transitions. This band gap behavior occurs because the intermolecular space decreases under compression, which increases the overlap between different groups of bands, and hence increases the charge overlap and delocalization in the system. However, in the pressure range 42–50 GPa, the band gap increases consistently with increasing pressure. This may be because a new, large, twelve-membered ring forms in this pressure range, which converts the whole molecule into a huge conjugated system, making the molecule more stable under compression. The variations in the band gap in different pressure ranges show different trends. The average decreases in the pressure ranges 0–7, 8–16, 17–24, and 25–41 GPa are 0.061 eV/GPa, 0.029 eV/GPa, 0.013 eV/GPa, and 0.004 eV/GPa, respectively. The average increase in the pressure range 42–50 GPa is 0.012 eV/GPa. This shows that the drop in energy is more pronounced in the low-pressure range than in the high-pressure region, in agreement with the results of previous studies of nitromethane under high pressure [44]. In the pressure range 0–20 GPa, the decrease in the band gap is 0.73 eV, which is smaller than the pressure-induced reduction in the band gap of HMX (1.05 eV) [22], but higher than that seen for nitromethane (0.23 eV) [44]. These very different reductions in the band gaps of the various materials may be due to different degrees of compressibility of their crystal structures in different pressure regions, which implies that the changes in electronic structure are in agreement with the above molecular geometry variations. In addition, the change in the band gap in

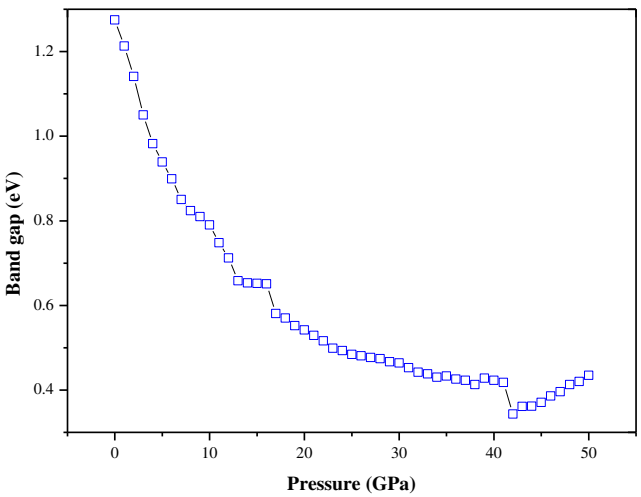

Fig. 7 Band gap of LLM-105 as a function of pressure

the range 8–16 GPa is not as consistent or regular as the changes seen in other pressure ranges (0–7, 17–24, 25–41, and 42–50 GPa), which are similar to the trends seen for the lattice constants and unit-cell angle in these pressure ranges. This indicates that the structure of the crystal is less ordered in the pressure range 8–16 GPa than in other pressure ranges.

Previous studies have reported the relationship between the band gap and the impact sensitivity for HMX [22], CL-20 [45], hexanitrostilbene [46], and heavy-metal azides [28]. Other investigations [47, 48] on the excitonic mechanism of detonation ignition show that the HOMO–LUMO (highest occupied molecular orbital to lowest unoccupied molecular orbital) gap in gas molecules that undergo shear strain, wave impact, or distortion can be related directly to the sensitivity. Our previous studies [22, 29] elucidated a first-principles band-gap criterion to measure impact sensitivity for a series of energetic crystals. For energetic crystals that have similar structures and similar thermal decomposition mechanisms, the smaller the band gap, the easier it is for electrons to transfer from the valence bands to the conduction bands, and the greater the potential of the material to decompose and explode. As can be seen in Fig. 7, the band gap of the crystal of LLM-105 gradually decreases with increasing pressure. Therefore, we can infer that the impact sensitivity of LLM-105 increases as the pressure rises.

To determine the bonding of the LLM-105 crystal at different pressures, its total density of states (DOS) and partial DOS (PDOS) at 0, 7, 8, 16, 17, 24, 25, 41, 42, and 50 GPa were calculated; these are shown in Fig. 8. The main features can be summarized as follows. (i) The DOS curve is characterized by several distinct peaks at 0 GPa, but the DOS peaks in the valence bands become more and more dispersed and have a tendency to shift to lower energies with increasing pressure. This indicates that band splitting and dispersion increases, accompanied by a broadening of the DOS, due to enhanced intermolecular interactions at high pressures. (ii) The DOS peaks in the valence and conduction bands near the Fermi level are dominated by the p states, which indicates that these p states play a very important role in the chemical reactions of LLM-105. (iii) The conduction bands have a tendency to shift to lower energies with increasing pressure in the range 0–42 GPa, which leads to a reduction in the band gap and showing the probability of electronic excitations, which is in good agreement with the conclusion drawn from the band-gap analysis. However, the behavior seen in the pressure range 42–50 GPa is different; in that range, the conduction bands have a tendency to shift to higher energies rather than to lower energies, resulting in an increase in the band gap, which agrees with the changes seen in the band gap in this pressure range.

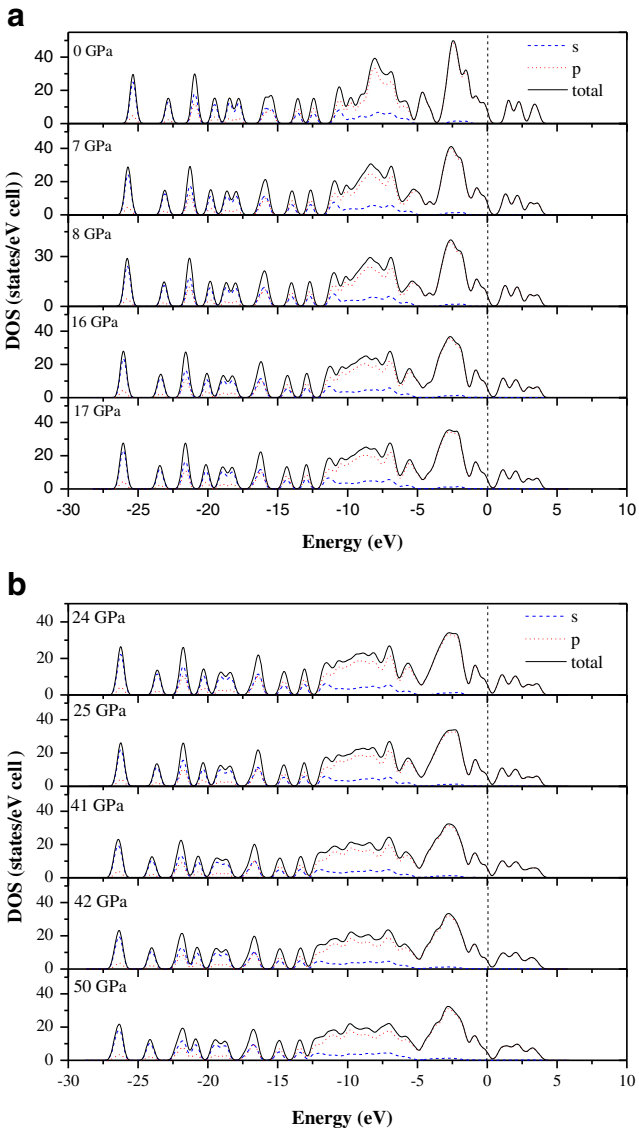

Fig. 8a–b TDOS of LLM-105 at **a** 0, 7, 8, 16, 17 GPa and **b** 24, 25, 41, 42, 50 GPa. The Fermi energy is shown as a *vertical dashed line*

Optical absorption spectra

In this section, we turn our attention to the optical absorption coefficients of the LLM-105 crystal at different pressures. The interaction of a photon with the electrons in the system can result in transitions between occupied and unoccupied states. The spectrum resulting from these excitations can be described as a joint density of states between the valence and conduction bands. The imaginary part $\varepsilon_2(\omega)$ of the dielectric function can be obtained from the momentum matrix elements between the occupied and unoccupied wavefunctions within the selection rules, and the real part $\varepsilon_1(\omega)$ of the dielectric function can be calculated from the imaginary part $\varepsilon_2(\omega)$ via the Kramers–Kronig relations. The absorption coefficient $\alpha(\omega)$ can be evaluated from $\varepsilon_1(\omega)$ and $\varepsilon_2(\omega)$ [49]:

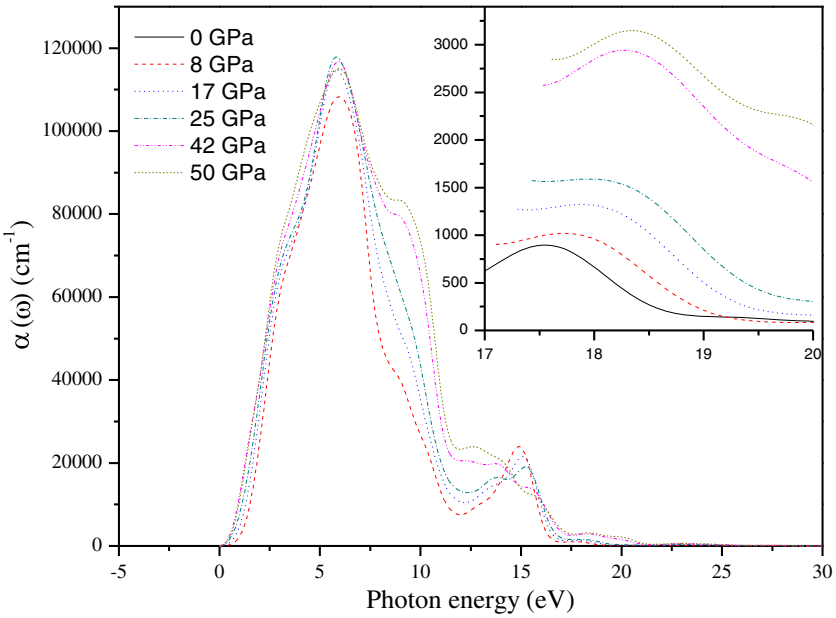

Fig. 9 Optical absorption spectrum of LLM-105 at different hydrostatic pressures

$$\alpha(\omega) = \sqrt{2}\omega\left(\sqrt{\varepsilon_1^2(\omega) + \varepsilon_2^2(\omega)} - \varepsilon_1(\omega)\right)^{1/2}. \quad (1)$$

The absorption coefficients $\alpha(\omega)$ of LLM-105 at different pressures are shown in Fig. 9. The absorption spectra show features in various regions corresponding to the molecular or lattice structures of the individual materials. The absorption spectra seen for LLM-105 at different pressures are qualitatively similar. They have an absorption band from 0 to 25.0 eV and exhibit more strong optical absorption from 2.5 to 18.5 eV. The magnitudes of the absorption coefficients of these peaks allow for an optical transition due to excitons. At ambient pressure, LLM-105 exhibits a relatively high absorption coefficient over a few closely spaced bands. The absorption bands from 13.1 to 17.2 eV correspond to the frequency of N–H stretching. It is found that the absorption at ~15 eV decreases with increasing pressure, which means that the N–H stretching weakens. This may be because the N–H bond lengths increase with increasing pressure, as observed in the molecular structure of LLM-105 under compression. The bands in the range 5.1–13.0 eV overlap, forming the strongest absorption region, which corresponds to N–O vibrations and ring distortion. In addition, Fig. 9 shows a new peak at 18.3 eV at a pressure of 42 GPa, which becomes more obvious at 50 GPa; this peak is due to O–H stretching. This peak from O–H stretching is not observed in the absorption spectrum of LLM-105 at ambient pressure, so the O–H bond may form at high pressure. The intermolecular H-bond lengths are less than 1.5 Å at 40 GPa or higher. Therefore, we can infer that the H-bonds have covalent character. As the pressure increases, the absorption peak of LLM-105 becomes wider and higher. In addition, LLM-105 has higher absorption coefficients at high pressure than at low pressure in the frequency region 0–12.5 eV, indicating a shift toward higher frequencies in the absorption spectrum. Overall, the absorption spectrum of LLM-105 displays more bonds—as well as stronger bands—in the fundamental absorption region at high pressure.

Conclusions

We performed a systematic study of the structural, electronic, and absorption properties of crystalline LLM-105 under hydrostatic pressures of 0–50 GPa utilizing density functional theory. Irregular changes in the lattice constants, unit-cell angles, bond lengths, bond angles, and band gap of LLM-105 were clearly observed, indicating that crystalline LLM-105 undergoes four structural transitions at 8, 17, 25, and 42 GPa, respectively. The structure is much stiffer in the *a*- and *c*-directions than in the *b*-direction, indicating that the compressibility of the LLM-105 crystal is anisotropic. The intramolecular H-bonds are strong in the pressure range 0–41 GPa but weaken in the range 42–50 GPa. The lengths of the intermolecular H-bonds gradually decrease with the increasing pressure until they are finally less than 1.47 Å, which means that the H-bonds have covalent character and tend to induce the formation of a new twelve-membered ring.

As the pressure increases from 0 to 42 GPa, the bad gap gradually decreases, except for two significant drops at 17 and 42 GPa that are caused by structural transformations, while it increases in a regular manner in the pressure range 42–50 GPa. An analysis of the DOS suggests that interactions between electrons, especially the valence electrons, are strengthened as the pressure is increased. The *p* states play a very important role in the chemical reactions of LLM-105.

The absorption spectrum of LLM-105 displays more—and stronger—bands in the fundamental absorption region at high pressure than at low pressure. A new absorption peak appears at 18.3 eV above 40 GPa. This peak is due to O–H stretching, indicating that there are covalent O–H bonds and a new twelve-membered ring in LLM-105.

Acknowledgments This work was supported by the National Natural Science Foundation of China (grant no. 21273115) and A Project Funded by the Priority Academic Program Development of Jiangsu Higher Education Institutions.

References

1. Millar RW, Philbin SP, Claridge RP, Hami J (2004) Propellants Explos Pyrotech 29:81–92
2. Liu H, Du HC, Wang GX, Liu Y, Gong XD (2012) J Mol Model 18: 1325–1331
3. Liu H, Wang F, Wang GX, Gong XD (2012) J Mol Model 18:4639–4647
4. Wang GX, Xiao HM (2007) Acta Chim Sinica 65:517–524
5. Hollins RA, Merwin LM, Nissan RA (1996) J Heterocycl Chem 33: 895–904
6. Turker L, Atalar T (2006) J Hazard Mater 137:1333–1344
7. Johnson MA, Truong TN (1999) J Phys Chem B 103:9392–9393
8. Pagoria P, Mitchell A, Schmidt R, Simpson R, Garcia F, Forbes J, Swansiger R, Hoffman D (1998) Synthesis, scale-up and characterization of 2,6-diamino-3,5-dinitropyrazine-1-oxide. Report UCRL-JC-130518. Lawrence Livermore National Laboratory, Livermore
9. Tran TD, Pagoria PF, Hoffman DM, Cutting JL, Lee RS, Simpson RL (2002) Characterization of 2,6-diamino-3,5-dinitropyrazine-1-oxide (LLM-105) as an insensitive high explosive. In: 33rd Int Annual Conf ICT, Karlsruhe, Germany, 25–28 June 2002
10. Wang YB, Ge ZX, Wang BZ, Ye ZH, Li YN, Shang Y (2011) Chin J Energ Mater 19:523–526
11. Ma HX, Song JR, Zhao FQ, Gao HX, Hu RZ (2008) Chin J Chem 26: 1997–2002
12. Averkiev BB, Antipin MY, Yudin IL, Sheremetev AB (2002) J Mol Struct 606:139–146
13. Gump JC, Stoltz CA, Mason BP, Freedman BG, Rall JR (2011) J Appl Phys 110:073523–073527
14. Li JS (2010) J Phys Chem B 114:2198–2202
15. Dreger ZA, Gupta YM (2010) J Phys Chem A 114:8099–8105
16. Dreger ZA, Gupta YM (2007) J Phys Chem B 111:3893–3903
17. Miao MS, Dreger ZA, Winey JM, Gupta YM (2008) J Phys Chem A 112:12228–12234
18. Munday LB, Chung PW, Rice BM, Solares SD (2011) J Phys Chem B 115:4378–4386
19. Ciezak JF, Jenkins TA, Liu ZX, Hemley RJ (2007) J Phys Chem A 111:59–63
20. Cady HH, Smith LC (1961) Studies on the polymorphs of HMX. Report LAMS-2653 TID-4500. Los Alamos National Laboratory, Los Alamos
21. Main P, Cobbledic RE, Small HRW (1985) Acta Crystallogr C 41: 1351–1354
22. Zhu WH, Xiao JJ, Ji GF, Zhang F, Xiao HM (2007) J Phys Chem B 111:12715–12722
23. Wu Q, Zhu WH, Xiao HM (2013) J Mol Model 19:4039–4047
24. Zhu WH, Zhang XW, Wei T, Xiao HM (2009) Theor Chem Acc 124: 179–186
25. Zhu WH, Zhang XW, Zhu W, Xiao HM (2008) Phys Chem Chem Phys 10:7318–7323
26. Zhu WH, Xiao JJ, Xiao HM (2006) Chem Phys Lett 422:117–121
27. Zhu WH, Xiao HM (2006) J Phys Chem B 110:18196–18203
28. Zhu WH, Xiao HM (2008) J Comput Chem 29:176–184
29. Zhu WH, Xiao HM (2010) Struct Chem 21:657–665
30. Wu Q, Zhu WH, Xiao HM (2013) J Phys Org Chem 26:589–595
31. Segall MD, Lindan PJD, Probert MJ, Pickard CJ, Hasnip PJ, Clark SJ, Payne MC (2002) J Phys Condens Matter 14:2717–2744
32. Vanderbilt D (1990) Phys Rev B 41:7892–7895
33. Kresse G, Furthmüller J (1996) Phys Rev B 54:11169–11186
34. Fletcher R (1980) Practical methods of optimization, vol 1. Wiley, New York
35. Ceperley DM, Alder BJ (1980) Phys Rev Lett 45:566–569
36. Perdew JP, Zunger A (1981) Phys Rev B 23:5048–5079
37. Gilardi RD, Butcher RJ (2001) Acta Crystallogr E 57:657–658
38. Zhu WH, Xiao HM (2009) J Phys Chem B 113:10315–10321
39. Zhu WH, Wei T, Zhu W, Xiao HM (2008) J Phys Chem A 112:4688–4693
40. Perdew JP, Chevary JA, Vosko SH, Jackson KA, Pederson MR, Singh DJ, Fiolhais C (1992) Phys Rev B 46:6671–6687
41. Liu Y, Zhang L, Wang GX, Wang LJ, Gong XD (2012) J Phys Chem C 116:16144–16153
42. Jeffrey GA (1997) An introduction to hydrogen bonding. Oxford University Press, New York
43. He WD, Zhou G, Wong NB, Tian AM, Long XP (2005) J Mol Struct (THEOCHEM) 723:217–222
44. Liu H, Zhao J, Wei D, Gong Z (2006) J Chem Phys 124:124501–124510
45. Xu XJ, Zhu WH, Xiao HM (2007) J Phys Chem B 111:2090–2097
46. Zhu WH, Shi CH, Xiao HM (2009) J Mol Struct (THEOCHEM) 910:148–153
47. Kuklja MM, Stefanovich EV, Kunz AB (2000) J Chem Phys 112: 3417–3423
48. Luty T, Ordon P, Eckhardt CJ (2000) J Chem Phys 117:1775–1784
49. Saha S, Sinha TP, Mookerjee A (2000) Phys Rev B 62:8828–8834